

# MIXED MODELS WITH $n > 1$ AND LARGE SCALE STRUCTURE CONSTRAINTS

S. A. Bonometto

Dipartimento di Fisica dell'Università & INFN sez. di Milano  
Via Celoria 16,  
I-20133 Milano, ITALY  
e-mail: bonometto@mil.infn.it

E. Pierpaoli

SISSA - International School for Advanced Studies, Via Beirut 2/4,  
I-34013 Trieste, ITALY  
e-mail: pierpa@sissa.it

---

## Abstract

Recent data on CBR anisotropies show a Doppler peak higher than expected in CDM cosmological models, if the spectral index  $n = 1$ . However, CDM and LCDM models with  $n > 1$  can hardly be consistent with LSS data. Mixed models, instead, whose transfer function is naturally steeper because of free-streaming in the hot component, may become consistent with data if  $n > 1$ , when  $\Omega_h$  is large. This is confirmed by our detailed analysis, extended both to models with a hot component whose momentum space distribution had a thermal origin (like massive neutrinos), and to models with a non-cold component arising from heavier particle decay. In this work we systematically search models which fulfill all constraints which can be implemented at the linear level. We find that a stringent linear constraint arises from fitting the extra-power parameter  $\gamma$ . Other significant constraints arise comparing the expected abundances of galaxy clusters and high- $z$  systems with observational data. If low values of  $\gamma$  are permitted, mixed models with  $1 < n < 1.4$  can have up to 45% of non-cold component, without violating any further linear constraint. Keeping to models with  $\gamma = 0.13$ , a suitable part of the space parameter still allows up to 30% of hot component (it is worth outlining that our stringent criteria allow only models with  $0.10 < \Omega_h < 0.16$ , if  $n = 1$ ). Spectra with  $n > 1$  are briefly discussed within the frame of inflationary theories. We also outline that models with such large non-cold component would ease the solution of the so-called baryon catastrophe in galaxy clusters.

PACS: 95.35; 98.80; 98.65 Dx; 98.62 L

Key words: cosmology theory, dark matter, large scale structure of the Universe.

---

## 1 Introduction

We need three kinds of ingredients to define a cosmological model: the background metric, the substance mix and the form of early departures from homogeneity. Background metric features are set by the density parameter  $\Omega = \Omega_{cr}$  and the Hubble parameter  $H = h 100 \text{ km s}^{-1} \text{ Mpc}^{-1}$  ( $\Omega$  is the average density and  $\Omega_{cr} = 3H^2/8\pi G$ ); the cosmic substance is fixed by partial density parameters, like  $\Omega_b = \Omega_b/\Omega_{cr}$  for baryons,  $\Omega_c = \Omega_c/\Omega_{cr}$  for cold dark matter (CDM), or  $\Omega_v$  for vacuum; finally, early deviations from homogeneity are described by the amplitude and the spectral index  $n$  of the initial fluctuation spectrum.

However, while early spectral features essentially do not depend on background and substance parameters, the linear evolution of the spectrum does and this is usually expressed through transfer functions  $T_z(k)$  ( $k = 2\pi/L$ ,  $L$  is the comoving length (scale), which give the ratio between the spectrum at a redshift  $z$  and its initial value.

In this paper we shall restrict ourselves to spatially flat models, with no residual vacuum energy, and focus on the interplay between the nature of the cosmic substance (yielding  $T_z$ ) and primordial spectral features, performing a systematic analysis of the amount and nature of hot dark matter (HDM), allowed by observational constraints, once we take the primordial spectral index (see below) in the range  $1 - n - 1.4$ .

In this work we shall however consider only large scale structure (LSS) features obtainable from linear theory, together with data on cosmic background radiation (CBR) anisotropies, which also refer to an epoch when fluctuations were still linear. The CBR temperature is almost direction independent and, once the dipole term (which accounts for the motion of Earth in respect to CBR) is subtracted, its fluctuations  $T(\hat{n}) = T_0 + \sum_{lm} a_{lm} Y_{lm}(\hat{n}) < 10^{-5}$ . Since we expect that deviations from a Gaussian behaviour are substantially absent at these stages, anisotropy features are suitably expressed through the quantities  $C_l = h^2 a_{lm}^2$ , for  $l \geq 2$ . As we shall see, CBR and LSS linear constraints already cause a severe selection among models and models to be used in numerical simulations should be submitted first to linear tests.

Let us now consider recent data on CBR anisotropies. As usual, we shall assume that the primordial spectrum reads

$$P(k) = A k^3 (xk)^{n-4} \quad (1.1)$$

( $x = x_o - x_{\text{rec}}$  is the distance from the recombination band, as  $x_o$  is the present horizon radius). It is then known (see, e.g.; Ma & Bertschinger 1996) that

$$C_l = (4\pi)^{-2} \int_0^z dk k^2 P(k) j_l^2(k; x_o) \quad (1.2)$$

with

$$j_l(k; x_o) = \int_0^{x_o} dx S(k; x) j_l[(x_o - x)k] \quad (1.3)$$

(Seljak & Zaldarriaga 1996). In this general expression, the source function  $S(k; x)$  contains contributions originating both at the last scattering band and along the path from it to us. For  $l = 1$  and low  $l$  (large scales  $L$ ), the most relevant effect is Sachs-Wolfe, and the simple form

$$C_l \approx (2\pi)^2 A \int_0^z (dk=k) (x_o k)^{n-1} j_l^2(x_o k) \quad (1.4)$$

can be used, which does not depend on the substance characteristics, but only on  $n$ . Although this approximation holds for rather small  $l$  only, in most cases the nature of the substance does not drastically affect the  $l$  dependence of  $C_l$  up to the so-called Doppler peak ( $l \approx 200$ ) (Dodelson et al. 1996).

Using eq. (1.4) and measuring  $C_l$  up to  $l \approx 30$ , the COBE collaboration (Bennett et al. 1996) could estimate the spectral index and found  $n = 1.2 \pm 0.3$ . Therefore, COBE data already favour  $n > 1$ , although they are fully compatible with  $n = 1$ .

More recent measurement (Netterfeld et al., 1997), extending up to  $l \approx 400$  (corresponding to angles  $\approx 0.5^\circ$ ), explored the doppler peak. The detected values seem to exclude models with low  $n$  values (Hancock et al. 1998), and agree with CDM and  $n = 1$  only for  $h = 0.3$  (Lineweaver 1997, Lineweaver & Barbosa 1998). An alternative possibility to fit such data is that  $n > 1$ .

Although these results obviously need further confirmation, they seem to tell us that inflation generated a spectrum  $P(k)$  with  $n > 1$ .

There are two main reasons why this is seen as a problem by some cosmologists. In the first place, the generic prediction of inflation is that  $n \approx 1$ . Section 4 will be devoted to a brief discussion on a class of inflationary theories which however predict  $n > 1$ . Furthermore, CDM fits with LSS improves for  $n < 1$ .

Another way to improve the fit of models with LSS consists into assuming that DM has also a hot component. The basic philosophy of mixed dark matter (MDM) models, since the first computation of their transfer function (Bonometto & Valdarnini, 1984; see also Achilli et al. 1985; Valdarnini & Bonometto 1985), is that the unexplored non-interacting world (gravitation

apart) can be quite complicated and probably contains several particle components. If one of them becomes non-relativistic when the scale  $L$  enters the horizon, then  $T$  is damped over all scales  $L < L_*$ . The detailed expression of  $T$  depends on the DM mix and the effect cannot be neglected if such component gives a substantial contribution to the overall density and  $L$  exceeds galaxy scales.

An attempt was also performed to consider  $n > 1$  in association to mixed DM (Lucchin et al. 1996), trying to balance opposite departures from standard CDM. However, the mix studied by these authors produces too many clusters, as was outlined by Borgani et al. (1996). Liddle et al. (1996) considered models with  $n > 1$ , in association with high  $h$  and possibly low  $h$  values, but they saw the same problems outlined by Borgani et al. (1996) and did not indicate an area of fit with data. If it is confirmed that  $n > 1$ , however, there seems to be no alternative to try to follow such pattern.

Owing to that, we tested a wide range of DM mixtures in association with values of  $n$  between 1 and 1.4. We found that the above difficulties can be overcome for a wide set of such models. Our analysis was restricted to the linear constraints described in sec. 3 and to models with  $\Omega_b = 0.1$ ,  $\Omega_c = 0$  and  $h = 0.5$ . Models were parametrized by  $h$  (the density parameter of the non-cold component) and  $d = z_{eq} = z_{der}$ ; here we defined  $z_{eq} \approx 10^4$ ; this would be the redshift when the photon density reaches the baryon+DM density, if all DM is CDM and  $\Omega = T = 2.733 K = 1$ . The derelativization redshift  $z_{der}$ , instead, occurs when the average particle momentum  $h_{pi} = m$  (particle mass).

A particle model allowing a continuous selection of  $[h; d]$  pairs is obtained if heavier particles ( $X$ ) decay into lighter massive particles ( $\nu$ ), whose phase-space distribution turns out to be quite different from usual massive  $\nu$ 's. Particle models leading to such hot DM component were discussed in several papers (e.g., Bonometto, Gabbiani & Masiero 1994, Ghizzardi & Bonometto 1996) and the evolution of density fluctuations in such context was discussed by Pierpaoli & Bonometto (1995) and Pierpaoli et al. (1996). Hereafter we shall distinguish these models from models with phase-space particle distribution of thermal origin, calling volatile their non-cold component. However we shall show that also a large deal of models based on massive  $\nu$ 's are consistent with linear constraints.

Owing to the peculiar phase-space distribution of volatile DM and to the actual energy dependence of fluctuation amplitudes in such models, public algorithms cannot be used to evaluate  $T$ . Here we shall make use of a flexible algorithm that we developed also to this aim. A discussion of phase-space distributions, fluctuation evolution and constraints arising from particle kinematics is given in sec. 2 and in Appendix A. More details on the algorithm are

given in Appendix B. As already mentioned, sections 3 and 4 deal with linear LSS constraints and inflationary theories yielding  $n > 1$ , respectively. Section 5 will be devoted to the analysis of results concerning acceptable models. We provide some plots showing the allowed area in the parameter plane and some sample transferred spectra. Furthermore, for parameter choices consistent with hot DM (e.g.: massive neutrinos), we compare the transferred spectra, finding small (expected) discrepancies between volatile models and those with massive 's. Section 6 is devoted to a final discussion and to conclusions.

## 2 Parameter space limitation

The substance of fixed models is made of various components, which can be classified according to their behaviour at the time when galactic masses enter the horizon. Particles which become non-relativistic before then, are said cold. There can be one or more of such components, indistinguishable through astrophysical measures. Tepid or warm components were sometimes considered (see, e.g.: Colombi et al. 1996; Pierpaoli et al., 1998), made of particles which become non-relativistic when small galactic scales ( $\sim 10^6 M_\odot$ ) have entered the horizon, but large galactic scales ( $\sim 10^{12} M_\odot$ ) still have not. Finally, hot component(s) are made of particles which become non-relativistic after the latter scale has entered the horizon.

Neutrinos, if massive, are a typical hot component. They were dynamically coupled to radiation down to a temperature  $T_{\text{rdg}} \approx 900 \text{ keV}$ . If their mass  $m_\nu$ , their number density, at any later time, is  $n_\nu = (3/4)g_\nu T^3$  (after electron annihilation  $T = T_{\text{rdg}} [a_{\text{rdg}} = a(t)] = (4/11)^{1/3} T$ , where  $T$  is radiation temperature) and their momentum distribution (normalized to unity) reads

$$f(p;t) = \frac{2}{3} \frac{(p^2 = T^3)}{(3) \exp[p = T(t)] + 1} \quad (2.1)$$

also when  $p \ll m_\nu$ . Henceforth, when  $T \ll m_\nu$ , their distribution is not thermal, although its shape was originated in thermal equilibrium. Notice that, for high  $p$ ,  $f$  is cut off as  $\exp(-p/T)$ .

Using the distribution (2.1) we can evaluate

$$h_{\text{pi}} = (7/4 = 1.75) T = 3.152 T \quad (2.2)$$

Accordingly,  $h_{\text{pi}} = m_\nu$  when  $T = 0.317 m_\nu$  and, for massive 's,

$$d = 5.2972 \cdot 10^{-4} (m_\nu = \text{eV}) \quad (2.3)$$

while

$$n_\nu = 2.1437 \cdot 10^2 g_\nu (m_\nu = \text{eV})^3 = 4h^2 \quad (2.4)$$

Hot components can also originate in the decay of a heavy particle  $X$ . Let  $N_{X, \text{d}g}$  be the comoving number density of  $X$ 's at their decoupling, taking place at some early time  $t_{\text{d}g}$ , well after they became non-relativistic, and let  $m_X$  be their mass. At  $t = t_{\text{d}g}$  their comoving number density reads:

$$N_X(t) = N_{X, \text{d}g} \exp[-(t - t_{\text{d}g})/a_{\text{d}y}] \quad (2.5)$$

with  $t_{\text{d}g} = a_{\text{d}y}$  (decay time). We shall assume a two-body decay process, as is more likely for dynamical reasons:

$$X \rightarrow \nu + \quad (2.6)$$

The decay gives rise to a light (volatile) particle  $\nu$ , of mass  $m_\nu = m_X$ , and to a massless particle  $\gamma$ . It can be either a photon ( $\gamma$ ) or a sterile scalar, as is expected to exist in theories where a global invariance is broken below a suitable energy scale (examples of such particles are familons and majorns). We shall show that the latter case (sterile scalar) is potentially more significant.

Once the decay process is over, the volatile momentum distribution reads:

$$\nu(p; t) = 2(Q = p) \exp(-Q) \quad \text{where} \quad Q = p^2/p^2 \quad (2.7)$$

and

$$p = (m_X/2) [a_{\text{d}y} = a(t)] \quad (2.7a)$$

provided that  $X$ 's, before they decay, never attain a density exceeding relativistic components. As is shown in Appendix A, this is avoided if the condition

$$h_d [1 + 2 = (1 + g = 8.3)]^{-1} \quad \text{for decay:} \quad (2.8)$$

is fulfilled. Here  $g$  refers to massless 's; e.g., for  $g = 6$ , eq. (2.14) yields  $h_d < 0.46$ . If matter domination occurs, the distribution (2.7) is distorted at small  $p$ , i.e. for particles originating in early decays. In this case the distribution can still be evaluated numerically, but no simple analytical expression can be given. Particles with large  $p$ , instead, were born in decays occurring when radiation domination was recovered and, therefore, the distribution is however cut off as  $\exp(-p^2/p^2)$ . The cut-off is therefore sharper than in the neutrino case.

Using the distribution (2.7), it is easy to see that the average

$$\langle p \rangle = (p^2 = 4) m_X a_{\text{d}y} = a(t) = p^2 = 2; \quad (2.9)$$

according to eq. (2.7a).  $\nu$ 's will therefore become non-relativistic when  $p = 2m_X$ ; henceforth

$$p = (2m_X) (z = z_{\text{eq}}) \quad (2.10)$$

(let us recall that we defined  $z_{\text{eq}} = 10^4$ ). Eq. (2.10) can be conveniently used in the distribution (2.7), instead of eq. (2.7a), as involves model parameters

( $m$  and  $d$ ), instead of early particle features ( $m_x$  and  $d_y$ ), which should be further elaborated in order to work out  $a_{dy} = a(d_y)$ .

Let us now discuss the decay patterns in more detail. First of all, if  $\tau > 10^7$ , the decay should occur at a redshift  $z > 10^7$ , so to avoid distortions of CBR spectrum (see, e.g.: Burigana et al., 1991). Two further possibilities should then be considered.

If the decay takes place before big bang nucleosynthesis (BBNS), the energy density of  $\nu$ 's is limited by the requirement that BBNS yields are consistent with observed nuclide abundances; henceforth the number of relativistic spin states  $g < 7$  (see, e.g.: Olive et al. 1997). Therefore, the actual limit on the energy density of  $\nu$ 's depends on the number of relativistic  $\nu$ 's at BBNS. If some  $\nu$  has a mass exceeding 1 MeV (particle data surely allow it for  $\nu_\tau$ ) and decays before decoupling,  $\nu$ 's can occupy its place during BBNS. As far as cosmology is concerned, differences between such volatile DM and ordinary hot DM would arise from the following 3 kinematic reasons: (i) the different phase space distribution of  $\nu$ 's in respect to massive  $\nu$ 's; (ii) the different energy dependence of fluctuation amplitudes; (iii) the allowed continuous range of HDM derelativization redshift; in the neutrino case, for a given HDM density, the derelativization redshifts are "quantized" by the discreteness of  $g$ .

By evaluating the transfer function for volatile models, we shall see that the points (i) and (ii) have a modest impact (see Table I in sec. 5). Consequences of (iii) would be important only if other cosmological parameters, like  $\Omega_b$  and  $h$ , were very well known. Altogether, therefore, the main differences induced by the above 3 points concern particle aspects. For example,  $\nu$ 's number density can be significantly smaller than  $\nu$ 's and their masses can be much greater. In spite of that, their density and derelativization redshift  $z_{der}$  can be equal and LSS effects are quite similar.

Let then still be  $\tau > 10^7$ , but let us assume that the decay occurs after BBNS; also in this case, there are constraints related to BBNS. In fact, decays produce an equal amount of  $\nu$ 's and  $\nu$ 's. The present CBR temperature normalizes abundance after the thermalization of decay photons. Accordingly, a large  $\nu$  density implies a small and massless  $\nu$  density before the decay. BBNS would therefore take place almost at the usual temperature, but earlier in time. Neutron decay would be therefore allowed a smaller time to work and neutron abundance, at the opening of the so-called Deuterium Bottleneck, would be greater. From this qualitative framework quantitative limits to the  $\nu$  abundance allowed by BBNS can be derived. We shall not further detail this point here and will only consider a softer limit, ensuing from the obvious requirement that the  $\nu$  density shall be smaller than  $\nu$  density, as the latter one has a "contribution" from "primordial"  $\nu$ 's. As is shown in Appendix A, for a model with given  $\Omega_h$  and  $d$ , at redshifts  $z > z_{der}$ , the following relation

holds:

$$h^2 = \frac{1}{1 + w_0} \frac{1}{h^2 d} \quad (2.11)$$

Henceforth, in this case, it must be

$$h^2 d < 1 \quad (\text{decay}) \quad (2.12)$$

Therefore, according to eq.(2.8), this case never implies primordial temporary matter-dominated expansion, at  $t < t_{\text{dy}}$ . It should be also outlined that these models can have quite a low massless neutrino density, as  $X$  decay increases temperature, but does not act on background. In Appendix A we show that

$$T = T_{\text{dec}} = (4/11)^{1/3} (1 - h^2 d) \quad (\text{decay}) \quad (2.13)$$

and a relevant variation of the massless sterile component (SM LC hereafter) can have a significant impact on  $T_z$ .

On the contrary, if  $\nu$ 's are sterile scalars and the decay takes place well after BBNS, constraints are not so stringent.  $\nu$ 's will behave just as massless  $\nu$ 's and these models can be characterized by a high SM LC density, which can also have a major impact in shaping the present LSS.

Therefore, significant constraints on the models can arise from this effect, which, however, cannot be discriminated a priori. Let us recall that, in the absence of  $X$  decay, the ratio  $\frac{1}{h^2} = 0.68132 (g = 6) w_0$ .  $X$  decay modifies it, turning  $g$  into an effective value

$$g_{\text{eff}} = g + (16/7) (11/4)^{4/3} h^2 d \quad (2.14)$$

(see appendix A). In this case, no matter dominance occurs before  $t_{\text{dy}}$  if

$$h^2 d < (1 + w_0)/2 \quad (\text{for sterile decay}) \quad (2.15)$$

and  $\nu$ 's contribution to the relativistic component lowers the equivalence redshift. When  $d(1 - h^2) > 1 + w_0$ , also  $\nu$ 's are still relativistic at equivalence. Accordingly, the equivalence occurs at either

$$z_{\text{eq}} = \frac{4h^2}{4} \frac{10^4}{1 + w_0 + h^2 d} \quad \text{or} \quad z_{\text{eq}} = \frac{4h^2}{4} \frac{10^4 (1 - h^2)}{1 + w_0 + 2 h^2 d} \quad (2.15)$$

in the former and latter case, respectively.

Mixed models involving a large volatile fraction, with late derelativization, are therefore allowed only within this scenario. In what follows we shall systematically analyze a large deal of mixed models, also with large  $h$  and  $d$ , consistent with this last picture, but we shall find that viable models with  $h^2 d > 1$  are not so frequent.



### 3 Linear constraints

Model parameters can be constrained from particle physics and/or from LSS. In this work we analyze a number of the latter constraints, which can be tested without discussing non-linear evolution.

More in detail, we shall consider the following prescriptions: (i) We set the numerical constant  $A$ , in the spectrum (1.1), so that  $C_2$  is consistent with COBE  $\pm 3\sigma$  intervals for  $Q_{rmsPS}$  (for different  $n$ 's).

(ii) Once the normalization is fixed at small  $k$ , we test the large  $k$  behaviour, first of all on the  $8h^{-1}Mpc$  scale. The mass  $M$ , within a sphere of radius  $L = h^{-1}Mpc$ , is

$$M = 5.96 \cdot 10^8 h^2 M_\odot \quad (\sigma_8=8)^3 : \quad (3.1)$$

Therefore, the cumulative cluster density

$$n(>M) = \frac{q}{2\pi} \frac{1}{(\sigma_8 M)^3} \int_{c=M}^{\infty} du [M = M(u)] \exp(-u^2/2) \quad (3.2)$$

for  $M = 4.2h^{-1} \cdot 10^8 M_\odot$  is directly related to the value of  $\sigma_8$ . In eq. (3.2) we take  $M(u)$  defined so that the mass variance (evaluated with a top-hat window function)  $\sigma_{M(u)}^2 = \sigma_c^2 u$ ;  $\sigma_c$  values from 1.69 (Peebles, 1980) to 1.55 were taken in figures 2 and 3.

Let us then consider  $N_{cl} = n(>M) (100h^{-1}Mpc)^3$  for the above  $M$  value. Optical and X-ray observations give a value of  $N_{cl}$  which is still not so different from 4, as found by White et al. (1993) and Biviano et al. (1993). Both the observational value and its theoretical prediction are however subject to a number of uncertainties. For instance, observations have some problems to fix cluster masses (see also below). From the theoretical side, non-linearity effects and mechanism turning fluctuations into clusters cannot be said to be completely under control. It is also wise recalling that  $N_{cl}$  and  $\sigma_8$  feel the slope of the spectrum, around  $8h^{-1}Mpc$ , in a slightly different way. Henceforth, we shall further comment on  $\sigma_8$  values, after discussing the spectral slope.

The above arguments tell us that, in our systematic search, it is wise to keep models with  $1 < N_{cl} < 10$ .

(iii) Models can survive the previous test for the whole range of  $A$  or for a part of it. Allowed  $A$  values were then used to evaluate the expected density parameters  $\rho_{gas} = \rho_{b, coll}$  in damped Lyman systems (for a review see Wolfe, 1993). Here

$$\rho_{coll} = \frac{p}{2} \text{erfc}\left[\frac{p}{\sigma_c} \sqrt{M(z)}\right]; \quad (3.3)$$

where  $\sqrt{M(z)}$  is the (top-hat) mass variance (form  $\sigma_{M(z)}$  at redshift  $z$ ) and

is an efficiency parameter which should be  $< 1$ . More specifically, using such expression, we evaluated  $D_{LAS}^{gas} = 10^3$ , taking  $z = 4.25$ ,  $\alpha_c = 1.69$  and  $M = 5 \times 10^{11} M_\odot$ .

This choice of values, as well as the choice of a top-hat window function, is a compromise among various suggestions in the literature, supported by different arguments. E.g., values of  $\alpha_c$  greater than 1.7 (Ma & Bertschinger 1994) or as small as 1.3 (Klypin et al. 1995) were discussed, a value of  $M$  ten times greater was often considered and the quantitative relevance of changing the window function was debated (see, e.g., Borgani et al., 1996 and Pierpaoli et al., 1996). According to Storrie-Lombardi et al. (1995), observations give  $D_{LAS} = 2.2 \pm 0.6$ . Therefore, we passed models only when  $D_{LAS} > 0.5$ . It must be outlined that varying this limit by a factor 2 would cause only marginal changes for models accepted. Slight shifts of  $\alpha_h$  or  $\alpha_d$  usually cause significant variation of  $D_{LAS}$  and this constraint turns out to be a fairly substantial one. Other tests concerning objects at large  $z$ , like early galaxies and QSO's, are less restrictive.

(iv) Bulk velocities were also evaluated and compared with POTENT reconstructions of velocity fields. Here we shall report no detail on the procedure, which causes no constraint, at the 2 $\sigma$  level.

On the contrary, a severe further selection arises from requiring that: (v) the extra-power parameter  $\gamma = 7.13 \times 10^3 (\sigma_{8,25})^{10/3}$  (here  $\sigma_{8,25}$  are mass variances on the scales  $R = 8.25 h^{-1} Mpc$ ) has values consistent with observations. From APM galaxies, Peacock and Dodds (1994) obtained  $\gamma = 0.23 \pm 0.04$ . In a more recent work, Borgani et al. (1997) give the interval  $0.18\{0.25$  obtained from the Abell/ACO sample. However, owing to the high value (10/3) of the exponent, a shift of  $\sigma_8$  by a small factor induces a major displacement. For example, if non-linear effects are underestimated by just 10%,  $\gamma$  increases by 37%. This effect is more likely for low  $\gamma$  values, which can be due to fairly high  $\sigma_8$  values. Henceforth we kept 0.27 as top acceptable value, which is both the upper limit given for APM and the 3 $\sigma$  upper limit for Abell/ACO. On the contrary we took 0.13 as lower limit, assuming that an underestimate of non-linear effects by 68% cannot be excluded.

As already mentioned, the constraint on  $\gamma$ , together with a suitable constraint on  $\sigma_8$ , implies a constraint on  $N_{cl}$ . Checks of  $\sigma_8$ ,  $N_{cl}$  and  $\gamma$  are, therefore, strictly related.

For instance, an observational value for  $\sigma_8$  can be deduced from X-ray data on the gas temperature  $T_g$  in galaxy clusters. If clusters are substantially virialized and the intracluster gas is isothermal, the mass  $M$  of a cluster can

be obtained, once the ratio

$$= \frac{\text{galaxy kinetic energy} = m \text{ ass}}{\text{gas thermal energy} = m \text{ ass}}$$

is known; then, the temperature function can be converted into a mass function, which can be fit to a Press & Schechter expression (see eq. 3.1), yielding the normalization of  $\Phi(M)$  (variance as a function of the mass scale  $M$ ) and hence  $\beta_8$ .

An alternative possibility, of course, amounts to deducing masses from galaxy velocities obtained from optical data. Both pattern imply some problem.

The value of  $\beta_8$  is currently obtained from numerical models. Henry & Aulmaud (1991), assuming  $\beta = 1.2$ , estimated  $\beta_8 = 0.59 \pm 0.02$  from a complete X-ray flux limited sample of 25 clusters they compiled. Various authors followed analogous patterns (see, e.g., White et al. 1993, Viana & Liddle 1996). Eke et al. (1996), adding observational uncertainties and error, claimed that  $\beta_8 = 0.50 \pm 0.04$ . An essential issue to obtain such result is that Navarro et al. (1995) simulations allow to take  $\beta = 1$  and an error  $< 6\%$ .

However, there seems to be a conflict between expected galaxy velocities, obtained assuming  $\beta = 1 \pm 0.06$  and optical data. In fact, the latter give a virial velocity dispersion in clusters  $\sigma_v \approx 800$  km/s, a value consistent with  $\beta > 1.5$  (Zabludov et al. 1990, Girardiet al. 1993).

It is possible that the critical assumption is that clusters are isothermal. In many clusters, cooling flows may play an important role and a fit to a cooling flow cluster with a simple isothermal model may yield a mean emission weighted temperature significantly reduced in respect to the virial value (see, e.g., Allen & Fabian 1998). However, according to Eke et al. (1998), cooling flows would cause a trend in disagreement with available data. More data on high  $z$  clusters are however needed to strengthen this statement. Other authors (Frenk et al. 1990, Borgani et al. 1997) claimed that the conflict between predicted and observed  $\sigma_v$  originates from contamination of optical data by groups accreting onto the clusters.

We can conclude that models with  $\beta_8$  in an interval  $0.45\{0.75$  should be viable. As expected, models passing previous tests keep comfortably inside such interval. The top  $\beta_8$  needed by models in g. 1b is 0.70 (for  $\beta_h = 0.26$ ,  $d = 1$ ,  $n = 1.2$ ) and the bottom  $\beta_8$  is 0.50 (for  $\beta_h = 0.18$ ,  $d = 16$ ,  $n = 1.2$ ). If the constraint on  $\beta$  is dropped (g. 1a), just two models with  $\beta_8 = 0.70$  (both yielding  $\beta < 0.10$ ) and a model with  $\beta_8 = 0.48$  ( $\beta_h = 0.22$ ,  $d = 16$ ,  $n = 1.3$ ,  $\beta = 0.11$ ) are added.

Some of the transferred spectra we obtain will be plotted, together with spec-

tral data obtained from Las Campanas survey (LCRS), kindly provided by Lin et al. (1996). It is however worth outlining soon that such comparison, although suggestive, is not so discriminatory.

A detailed description of LCRS is given by Schectman et al. (1996). The survey encloses  $3 \times 3$  "slices"  $1^\circ:5' - 8^\circ$  wide, in the northern and southern hemispheres. Data were taken using two multi fiber systems. Fields  $1^\circ:5' - 1^\circ:5'$  wide were inspected above suitable photometric limits, chosen so that there were more galaxies per field than available fibers. Then, target galaxies in each field were randomly selected and a "field sampling factor"  $f$  was memorized, to be used in any further statistical analysis. The average values of  $f$  are different for the two multi fiber systems, which are able to inspect 50 and 112 objects, and amount to 0.58 and 0.70, respectively. The nominal photometric limits are also different for the two systems, amounting to  $16 \text{ m} - 17.3$  and  $15 \text{ m} - 17.7$ , respectively. A further geometric effect is due to the impossibility to inspect galaxies, in a given field, if nearer than  $55''$ .

The actual situation for power spectrum measurement from LCRS appears to fall into two regimes. On scales  $L < 80 \{ 100 h^{-1} \text{Mpc} \}$  ( $k > 0.2 h$ ) a fair determination of the spectrum is obtained. In this range, LCRS results strengthen results from other surveys. Larger scales would be more discriminatory, but here errors are greater and the sample variance might cause further shifts.

When compared with such observational spectra, a reasonable transferred spectrum should lie below observational errorbars, up to  $80 \{ 100 h^{-1} \text{Mpc} \}$ ; the gap between theoretical and observational spectra is related to the amount of bias (constant gap means a scale independent bias level). For  $k$  values much beyond this scale, requiring a detailed  $\chi^2$  may be excessive. Although there are mixed models which provide it, we see no reason to disregard models whose spectrum falls within  $\pm 3$  errorbars from the reconstructed spectrum. An example of such models are  $\Lambda$ CDM models, with various  $\Omega_m$  contents, which were shown also by Lin et al. (1996), but not treated in this article.

The basic issue following this discussion, which can be suitably rephrased for other data sets, is that it is non-trivial to extract discriminatory criteria from observational spectra. Most of such criteria are expressed by quantities already introduced earlier in this section. Furthermore, quite in general, in a systematic search, predictions are to be met with fairly wide observational intervals. In fact, a marginal agreement with the data, for a model met in a systematic analysis, can be often improved by a suitable finer tuning of parameters. We verified that, in several cases, this was the actual situation.

#### 4 Inflationary models yielding $n > 1$

This section is a quick review of results in the literature, aiming to show that there is a wide class of inflationary models which predict  $n > 1$ , but  $< 1.4$ . It can be therefore skipped by those who are aware of such results.

Density perturbations arise during inflation because of quantum fluctuations of the inflaton field  $\phi$ . Their amplitude and power spectrum are related to the Hubble parameter  $H$  during inflation and to the speed  $\dot{\phi}$  of the slow {rolling} down process, along the scalar field potential. It can be shown that the critical quantity is the ratio  $W(k) = H^2/\dot{\phi}$ , where  $H$  and  $\dot{\phi}$  are taken at the time when the scale  $2\pi/k$  leaves the event horizon. The value of the spectral index can then be shown to be

$$n = 1 + 2 \frac{d(\log W)}{d(\log k)} \quad (4.1)$$

and, if  $W$  (slowly) decreases with time, we have the standard case of  $n$  (slightly) below unity (it should be reminded that greater scales flow out of the horizon at earlier times). This decrease is due to an acceleration of the downhill motion of  $\phi$  and an opposite behaviour occurs if  $\dot{\phi}$  decreases while approaching a minimum. The basic reason why a potential yielding such a behaviour seems unappealing, is that the very last stages of inflation should rather see a significant  $\phi$  field acceleration, ending up into a regime of damped oscillations around the true vacuum, when reheating occurs.

These objections can be overcome if the usual perspective is reversed: reheating does not arise when an initially smooth acceleration naturally grows faster and faster, as the slope of the potential steepens; on the contrary, reheating starts abruptly, thanks to a first order phase transition, perhaps to be identified with the break of the GUT symmetry. Before such transition and since the Planck time, most energy content naturally resided in potential terms, so granting a vacuum dominated expansion. This picture of the early stage of the cosmic expansion is the so-called hybrid inflation, initially proposed by Linde (1991a).

A toy model realizing such scenario (Linde 1991b, 1994) is obtained from the potential

$$V(\phi; \chi) = (\phi^2 - \phi_0^2)^2 + 2g^2\phi^2\chi^2 + m^2\chi^2 \quad (4.2)$$

depending on the two scalar fields  $\phi$  and  $\chi$ , expected to be slowly and fastly evolving, respectively. If the slowly evolving field is embedded in mass terms, the potential reads

$$V(\phi) = M^2\phi^2 + \phi^4 + \chi^4 \quad (4.3)$$

where

$$\chi^4 = \chi^4 + m^2\chi^2 \quad \text{and} \quad M^2 = 2(g^2\phi^2 - \phi_0^2) : \quad (4.4)$$

Eq. (4.3) shows that  $V$  has a minimum at  $\phi = 0$ , provided that  $M^2 > 0$ . If  $M^2 < 0$ , instead, the minimum is for  $\phi = \sqrt{-M^2/2}$ , yielding  $n = 1$  when  $\phi = 0$ .

Large  $\phi'$  values therefore require that  $\phi$  vanishes and then the potential

$$V(\phi'; 0) = \frac{1}{4} \phi'^4 + m^2 \phi'^2 \quad (4.5)$$

allows a Planck time inflation, as  $\phi'$  rolls downhill taking  $V$  from an initial value  $\frac{1}{4} \phi_1'^4$  to  $\frac{1}{4} \phi'^4$ . This downhill motion is expected to decelerate when the second term at the r.h.s. of eq. (4.5) becomes negligible in respect to  $\frac{1}{4} \phi'^4$ , which essentially acts as a cosmological constant. This deceleration abruptly breaks down when the critical value  $\phi'_c = \sqrt{m^2} = g$  is attained, for which  $M^2$  changes sign. At that point the configuration  $\phi = 0$  is unstable and the transition to the true vacuum configuration reheats (or heats) the Universe.

There are a number of constraints to the above picture, due to the requirements that at least 60 e-foldings occur with  $\phi' > \phi'_c$  and that fluctuations have a fair amplitude. Such constraints are discussed in several papers (see, e.g., Copeland et al. 1994, and references therein) and cause the restriction  $n < 1.4$ . Henceforth, in this work we shall debate models with  $1 < n < 1.4$ .

Let us however outline that hybrid inflation is not just one of the many possible variations on the inflationary theme. In spite of the apparent complication of the above scheme, it is an intrinsically simple picture and one of the few patterns which can allow to recover a joint particle/astrophysical picture of the very early Universe, as was naturally hoped before it became clear that the Higgs field of the GUT transition could not be the inflaton (see, e.g., Sha & Vilenkin, 1984 and Pi, 1984).

## 5 Transfer functions and spectra

Any realistic cosmological model is expected to contain baryons (density  $\rho_b = \rho_{b,cr}$ ), photons (present temperature  $T_0 = 2.733$  K, density  $\rho_\gamma$ ), CDM (density  $\rho_c = \rho_{c,cr}$ ) and a SM LC. The basic SM LC are the usual 3 massive  $\nu$ 's.

Mixed models include also a HDM component (density  $\rho_h = \rho_{h,cr}$ ) and the SM LC is however modified. If HDM particles are massive  $\nu$ 's, SM LC density is lower, or even vanishing when all  $\nu$ 's are massive (of course, sterile massless particles can be however added ad hoc). In the volatile case, we face the opposite situation, as the SM LC must contain at least a scalar, in top of usual massless  $\nu$ 's. In all cases, we can parametrize SM LC by using  $w = 0.68132$  ( $g_{eff}=6$ ), according to eq. (2.14).

The algorithm used to evaluate the transfer functions of a wide range of mixed models is discussed in Appendix B and, besides of allowing any value of  $\rho_b$ ,  $\rho_h$ ,  $w$  and other standard parameters, allows to arbitrarily the expression

of  $\langle p \rangle$  [see eqs. (2.1) and (2.7)] and the dependence on  $p$  of the amplitude of HDM fluctuations.

As already mentioned, however, in this work  $\omega = 1$ ,  $\beta = 0$ ,  $H = 50 \text{ km s}^{-1} \text{ Mpc}^{-1}$  and  $\sigma_8 = 0.1$  (some plots for them also models, with different values of  $\sigma_8$  are however shown). Exploring other values of the former 2 parameters would amount to extending the physical range of models. The expected behaviour for different values of the latter two parameters, instead, can be qualitatively inferred from the results shown below. A test of the effect of varying them should be focused onto a portion of the parametric space, selected on the basis of the results of this work and other physical criteria.

Within the above restrictions, we tested models at regular logarithmic interval for  $z_{\text{der}}$ , taking  $\log_2 d = 1; \dots; 5$  (7 values) and at regular interval for  $\log_2 \rho_{\text{hot}}$ , taking  $\rho_{\text{hot}} = 0.10; 0.12; \dots; 0.44$ ; and  $0.45$  (19 values). A non-systematic sampling of this parameter space allowed us to exclude some models a priori, reducing the total exploration to 120 models.

There is a significant overlap between these values of  $\rho_{\text{hot}}$  and  $d$  and those allowed in mixed models with massive  $\nu$ 's, as can be seen also in Fig. 1 here-below. One of our basic aims was then to obtain a quantitative estimate of the impact of the different momentum distribution on transfer functions. To this aim we re-evaluated  $T$ , for a few mixed models with HDM made either by massive neutrinos or volatiles, but with the same values of  $\rho_{\text{hot}}$ ,  $d$  and  $g_{\text{eff}}$ , according to eqs. (2.3), (2.4), (2.14). The results of this comparison for two model sets are shown in Table I.

The detection of the (modest) amount of such shifts is one of the results of this work. However, this does not decrease the relevance of volatile models, as they allow parameter choices which, otherwise, would be impossible with the standard 3 flavours. Furthermore, these models require and allow a high level of SMLC.

The main output of this work is however represented by Fig. 1(a,b), where we show which parts of the parameter space are compatible with linear constraints, for spectral indices  $n = 1; 1.1; \dots; 1.4$ .

Fig. 1b takes into account all the constraints mentioned in sec. 3. Models inside the curves fulfil the requirements on COBE quadrupole value (3 intervals), galaxy clusters, high- $z$  objects and  $\dots$ . On the contrary, Fig. 1a excludes the requirement on  $\dots$ . Models forbidden by Fig. 1b but allowed by Fig. 1a should be accurately tested for in non-linear simulations.

For most models considered, the spectrum

$$P(k) = A k^n T^2(k); \quad (5.1)$$

Table 1

Ratio between transfer functions in volatile and thermal models ( $T_{\text{vol}}/T_{\text{ther}}$ ) at various comoving scales for different components. The upper part refers to models with  $h = 0.3$  and 3 massive neutrinos, the lower part to models with  $h = 0.1$  and 1 massive neutrino. In both cases  $\Omega_m = 1$ ,  $h = 0.5$  and  $\Omega_b = 0.1$ .

L/Mpc	cold	hot	baryons	total
0.2000E+05	1	1	1	1
0.5120E+03	1	1	1	1
0.2048E+03	0.9995E+00	0.9996E+00	0.9995E+00	0.9995E+00
0.8192E+02	0.1001E+01	0.1002E+01	0.1001E+01	0.1001E+01
0.3277E+02	0.1003E+01	0.1004E+01	0.1003E+01	0.1003E+01
0.1311E+02	0.1003E+01	0.1004E+01	0.1003E+01	0.1003E+01
0.5243E+01	0.1005E+01	0.1003E+01	0.1005E+01	0.1004E+01
0.2097E+01	0.1007E+01	0.1012E+01	0.1007E+01	0.1009E+01
0.8389E+00	0.1006E+01	0.1036E+01	0.1006E+01	0.1015E+01
0.2000E+05	1	1	1	1
0.5120E+03	1	1	1	1
0.2048E+03	0.9995E+00	0.9996E+00	0.9995E+00	0.9995E+00
0.8192E+02	0.1001E+01	0.1001E+01	0.1001E+01	0.1001E+01
0.3277E+02	0.1003E+01	0.1002E+01	0.1003E+01	0.1003E+01
0.1311E+02	0.1003E+01	0.1002E+01	0.1003E+01	0.1003E+01
0.5243E+01	0.1005E+01	0.1001E+01	0.1005E+01	0.1005E+01
0.2097E+01	0.1007E+01	0.1008E+01	0.1007E+01	0.1007E+01
0.8389E+00	0.1006E+01	0.1026E+01	0.1006E+01	0.1008E+01

where the constant

$$A = \frac{2}{9} x_0^{n+3} A ; \quad (52)$$

starts at low  $k$ 's with values similar to standard CDM. If  $n > 1$ , it soon abandons CDM behaviour, rising in a slightly steeper way. Both for  $n > 1$  and  $n = 1$ , however, its bending at maximum is sharper. At the rhs of the maximum it returns below CDM. At large  $k$ 's ( $> 1 \text{ Mpc}^{-1}$ ), its decrease, sometimes, is (slightly) less steep than CDM.

Some examples of such behaviour are given in fig. 2 for volatile models and in fig. 3 for thermal models; all cases we show have  $n > 1$ . Models are compared with CDM (dotted curve) and with the spectrum reconstructed by Lin et al (1996) from LCRS data (3 errorbars). Models are ordered with increasing



$h$ . For volatile models, various values of  $d$  are considered, including high values; in particular, in fig. 2c we show a spectrum obtained with  $z_{\text{der}} = 625$ .

Massive neutrino models obviously have  $w < w_0$ . Extra SM LC can be however added ad hoc and the comparison of Table I was made after implementing  $w$  to the value of volatile models. The boundaries shown in fig. 1 are also valid when all SM LC expected in a volatile model is included. Its presence causes a later transition from radiation dominated to matter dominated expansion. As a consequence, the peak of the transferred spectrum is shifted to smaller  $k$ 's and, in general, this favours the agreement of models with linear constraints.

While the boundaries marked in fig. 1 therefore apply to neutrino models with extra SM LC, the spectra shown in fig. 3(a,b) are for physical models without extra SM LC. The spectrum in fig. 3c, instead, is obtained adding an amount of SM LC corresponding to 3 massless  $\nu$ 's.

The inverse transfer functions  $T_p^{-1}$  of all models considered, were also parametrized with 4th degree polynomials in  $\ln k$ , both for  $z = 0$  and  $z = 425$ . The table of coefficients will be made available upon request.

## 6 Discussion

After evaluating the transfer function of a set of more than 120 fixed models, with  $\Omega_b = 1$  and  $h = 0.5$ , we obtained the expected values of several observable quantities, which can be estimated using the linear theory. In particular we worked out the expected cluster number density, the abundance of Damped Lyman  $\alpha$  clouds, the mass variances at 25 and 8  $h^{-1} \text{Mpc}$ . From them we also estimated the extra power parameter  $\sigma_8$ .

The HDM of the models we considered was either thermal (massive  $\nu$ 's) or volatile (arising from heavier particle decay). We discussed the parameter space for the latter case and compared the transfer functions for thermal and volatile HDM, for values of  $h$  and  $d$  which allow both models. Differences between thermal and volatile models are then really significant only as far as the expected SM LC is concerned.

Results on parameter constraints are summarized in figures 1 (a,b). As was already known, a number of such models with  $h$  up to 0.30 pass the above tests. If  $n = 1$ , volatile models allow little extra freedom, namely for high  $z_{\text{der}}$ . The situation is already different for  $n \neq 1$ . Here models with  $z_{\text{der}} \neq 600$  are allowed for  $h$  up to 0.14 and greater  $h$  are allowed for values of  $z_{\text{der}}$  still much lower than those allowed by neutrino models. The range of  $h$  values allowed with  $z_{\text{der}} \neq 600$  extends upwards as  $n$  increases and overcomes 0.20 for

$n = 1.4$ . The greatest value found for  $h$  is 0.30 for  $z_{\text{der}} = 10^4$  with  $n = 1.2$ . Thermal models with 2 or 3 massive neutrinos and a suitably added SM LC arrive to  $h \approx 0.28$ , for  $n = 1.2$  and  $n = 1.3$ , respectively.

These values may not seem too large, in respect to  $h$  values currently used in the literature (with thermal models). It must be outlined, however, that our acceptance criteria are more stringent than usual. With such criteria, no thermal model with  $h > 0.16$  is accepted for  $n = 1$ .

Let us also draw the attention on the very low values of  $z_{\text{der}}$  that volatile models with large  $n$  allow. As an example of low  $z_{\text{der}}$ , in g. 2c we show the transferred spectrum of a model with 22% of HDM and  $z_{\text{der}} = 625$ , which, for a fairly high value of COBE quadrupole, has excellent fits with all linear constraints. HDM particles of this and similar models have a mean square velocity  $\approx 500$  km/s today, still away from potential wells. Such speed is likely to guarantee them not to cluster with baryon or CDM on any scale. Dynamical mass estimates, in a world containing such component, might lead to observe 75{80% of critical density.

It should be also mentioned that, if the constraint on  $z_{\text{der}}$  is dropped, greater  $h$ 's seem allowed (see g. 1a). The top value we found is  $h = 0.45$  with  $z_{\text{der}} \approx 5000$ . With 3 or 2 massive neutrinos the highest  $h$  obtainable are 0.40 and 0.38, respectively. As already outlined, in g. 1 neutrino model curves are overlapped to volatile model parameter space, but the allowed regions apply to them only after adding suitable SM LC.

Liddle et al. (1996), in a paper focused on  $n = 1$  models, mentioned that a model with  $h = 0.35$ ,  $n = 1.2$ ,  $h = 0.4$  agreed with the linear constraints they imposed. Using our linear constraints,  $h$  is to be lowered to  $\approx 0.30$ . Volatile models do not need to lower  $h$  so far, to agree with data, as they naturally have SM LC, which induces fairly similar effects. Also thermal models can agree with data keeping to  $h = 0.5$ , rising  $n$ , with or without extra SM LC. Fig. 3 illustrates some spectra for such models.

Models with high HDM content and high average kinetic energy, could also ease the problem of the apparent baryon excess in several galaxy clusters. It has been known for several years (see, e.g., White & Frenk 1991, Boehringer et al. 1992, Briel et al. 1992, David et al. 1993, White et al. 1993) that the baryon mass fraction in galaxy clusters is high, in respect to expectations in flat, pure CDM models. According to White et al. (1993), even neglecting baryons in galaxies, the observed baryon fraction yields

$$\Omega_b h^{3=2} = 0.05 \pm 0.02 \quad (6.1)$$

for flat, pure CDM models. BBNS limits of Walker et al (1991) required then that  $\Omega_b h^2 = 0.0125 \pm 0.0025$ .

Much work was then performed to analyze individual clusters and lists of baryon contents in cluster samples were presented by several authors (see, e.g., White & Fabian, 1995). The situation is summarized in a recent paper by Evrard (1997) who obtains the constraint

$$\Omega_b h^{3/2} = 0.060 \pm 0.003 \quad (6.2)$$

This is to be taken with recent BBNS limits on  $\Omega_b$ . E.g., Copi et al (1995) give  $0.007 < \Omega_b h^2 < 0.024$  and therefore  $\Omega_b < 0.1$ , with  $h = 0.5$  is marginally allowed. For  $h = 0.5$ , as we assumed here, eq. (6.2) gives a central value  $\Omega_b = 0.17$  and a 3  $\sigma$  minimum  $\Omega_b > 0.14$ .

If HDM does not cluster with CDM and baryons, a measure of  $\Omega_b$  would however yield  $\Omega_{b,app} = \Omega_b (1 - \Omega_h)$ . Within mixed models, therefore, agreement with data requires  $\Omega_h > 0.41$  or  $> 0.29$ , respectively. We have shown in this work that the latter value is coherent with LSS constraints, if  $1.2 < n < 1.4$ ; as  $n$  increases, compatible models have  $z_{der}$  values decreasing, down to  $\sim 2500$ .

Limits become more permissive if masses obtained from lensing are replaced to those obtained from X-ray data (see, e.g., Allen & Fabian 1998). High baryon density, however, seems a widespread feature. Perhaps the limits shown in eq. (6.2) are to be reset, taking greater cluster masses, but, if  $\Omega_0 = 1$ , there seems to be a definite evidence of a component which tends not to cluster with CDM. The debate is related to the discussion on  $\Omega_8$  limits in sec. 3.

In the literature, mixed models with  $n = 1$  were often considered and allow to predict acceptable values of a number of observable quantities, if low rates for the HDM component are taken. Considering  $n > 1$  is at least as legitimate as taking  $n < 1$  and leads to a range of mixed models allowing fair predictions on the same quantities. We showed that models with  $n > 1$  require and allow higher HDM contents. They could therefore improve our understanding of why  $\Omega_0$  measures seem to give increasing values when greater scales  $L$  are considered. This was one of the basic motivations to introduce mixed models, more than a decade ago.

#### Acknowledgements

Thanks are due to Stefano Borgani for discussions. E.P. wishes to thank the Department of Physics of the University of Milan for its hospitality during part of the preparation of this work. E. Bertschinger, who refereed this paper, is to be gratefully thanked for a number of useful suggestions. Thanks are also due to H. Lin, who kindly gave us points and errorbars for the LCRS spectrum.

## References

- Achilli S., Occhionero F. and Scaramella R., (1985), *Astrophys. J.* 299, 577  
 Allen S.W. and Fabian A.C. (1998) *astro-ph/9802219*  
 Barandela F., Einasto J., Gottloeber S., Mueller V. and Starobinski A. (1997) (preprint)  
 Bennet C.L. et al. (COBE collaboration) (1996), *Astrophys. J.* 464, L1  
 Biviano A., Girardi M., Giuricin G., Mardirossian F. and Muzzetti M. (1993) *Astrophys. J.* 411, L13  
 Bonometto S.A., Gabbiani F. and Masiero A. (1994) *Phys. Rev. D* 49, 3918  
 Bonometto S.A. and Valdarnini R. (1984) *Phys. Lett. A* 103, 369  
 Borgani S., Gardini A., Girardi M. and Gottloeber S. (1996) *Mon. Not. R. A. S.* 280, 749  
 Borgani S., Lucchin F., Matarrese S. and Moscardini L. (1996) *Mon. Not. R. A. S.* 280, 749  
 Borgani S., Moscardini L., Plionis M., Gorski K.M., Holzmann J., Klypin A., Primack J.R., Smith C.C. and Stompor R. (1997) *New Astr.* 321, 1  
 Broadhurst T.J., Ellis R.S., Koop D.C. and Szalay A. (1990) *Nature* 343, 729  
 Burigana C., De Zotti G. and Danese L. (1991) *Astrophys. J.* 379, 1  
 Carr B.J. and Lidsey J. (1993) *Phys. Rev. D* 48, 543  
 Colombi S., Dodelson S. and Widrow L.M. (1996) *Astrophys. J.* 458, 1  
 Copeland E.J., Liddle A.R., Lyth D.H., Stewart E.D. and Wands D. (1994) *Phys. Rev. D* 49, 6410  
 Copi C.J., Schramm D.N. and Turner M.S. (1995) *Science* 267, 192  
 Dodelson S., Gates E. and Stebbins A., (1996) *Astrophys. J.* 467, 10  
 Einasto J., Einasto M., Gottloeber S., Mueller V., Saar V., Starobinski A., Tago E., Tucker D., Andemach H. and Frisch (1997) *Nature* 385, 139  
 Eke V.R., Cole S. and Frenk C.S. (1996) *Mon. Not. R. A. S.* 282, 263  
 Eke V.R., Cole S., Frenk C.S. and Henry J.P. (1998) *astro-ph/9802350*  
 Evrard A.E. (1997) *Mon. Not. R. A. S.* 292, 289  
 Frenk C.S., White S.D.M., Efsthathiou G. and Davis M. (1990) *Astrophys. J.* 351, 10  
 Gaztanaga E. and Baugh C.M. (1997) *astro-ph/9704246*  
 Ghizzardi S. and Bonometto S.A., (1996) *A & A* : 307, 697  
 Girardi M., Biviano A., Giuricin G., Mardirossian F. and Muzzetti M. (1993) *Astrophys. J.* 404, 38  
 Hancock S., Rocha G., Lasenby A.N. and Gutierrez C.M. (1998), *Mon. Not. R. A. S.* 294, L1  
 Henry J.P. and Aulard K.A. (1991) *Astrophys. J.* 372, 410  
 Klypin A., Borgani S., Holtzman J. and Primack J.R. (1995) *Astrophys. J.*

444, 1

- Landy S.D., Shectman S.A., Lin H., Kirshner R.P., Oemler A.A. and Tucker D. (1996) *Astrophys. J.* 456, L1
- Liddle A.R., Lyth D.H., Schaefer R.K., Sha Q. and Viana P.T.P. (1996) *Mon. Not. R.A.S.* 281, 531
- Lin H., Kirshner R.P., Shectman S.A., Landy S.D., Oemler A., Tucker D.L. and Schechter P. (1996) *Astrophys. J.* 471, 617
- Lineweaver C. (1997) *astro{ph/9702040}*
- Lineweaver C. and Barbosa D. (1998) *Astrophys. J.* 496 (in press).
- Linde A. (1991a) *Phys. Lett. B* 249, 18
- Linde A. (1991b) *Phys. Lett. B* 259, 38
- Linde A. (1994) *Phys. Rev. D* 49, 748
- Lucchin F., Colafrancesco S., De Gasperis G., Matarrese S., Mei S., Mollerach S., Moscardini L. and Vittorio N. (1996) *Astrophys. J.* 459, 455
- Ma C.P. and Bertschinger E. (1994) *Astrophys. J.* 434, L5
- Ma C.P. and Bertschinger E. (1995) *Astrophys. J.* 455, 7
- Mollerach S., Matarrese S. and Lucchin F. (1994) *Phys. Rev. D* 50, 4835
- Netterfeld C.B., Devlin M.J., Jarosik N., Page L. and Wollack E.J. (1997) *Astrophys. J.* 474, 47
- Oliver K., Steigman G. and Skillman E. (1997) *Astrophys. J.* 483, 788
- Peacock J.A. and Dodds S.J. (1994) *Mon. Not. R.A.S.* 267, 1020
- Peebles P.J.E. (1980), *The Large Scale Structure of the Universe*, Princeton University Press, Princeton.
- Pis Y. (1984) *Phys. Rev. Lett.* 52, 1725
- Pierpaoli E. and Bonometto S.A. (1995) *A & A*: 300, 13
- Pierpaoli E., Coles P., Bonometto S.A. and Borgani S. (1996) *Astrophys. J.* 470, 92
- Pierpaoli E., Borgani S., Masiero A. and Yamaguchi M. (1998) *Phys. Rev. D* 57, 2089
- Seljak U. and Zaldarriaga M. (1996) *Astrophys. J.* 469, 437
- Sha Q. and Vilenkin A. (1984) *Phys. Rev. Lett.* 52, 691
- Shectman A.S., Landy S.D., Oemler A., Tucker D.L., Kin H., Kirshner R.P. and Schechter P.L. (1996) *Astrophys. J.* 470, 172
- Storrie-Lambers J., McMahon R.G., Irwin M.J. and Hazard C. (1995) *Proc. ESO Workshop on QSO A.L. & astro{ph/9503089}*
- Valdmini R. and Bonometto S.A. (1985), *A & A*: 146, 235
- Viana P.T.P. and Liddle A.R. (1996) *Mon. Not. R.A.S.* 281, 323
- Walker T.P., Steigman G., Schramm D.N., Olive K.A. and Kang H. (1991) *Astrophys. J.* 376, 51

White S D M ., Efstathiou G .and Frenk C . (1993) M on. Not. R A S. 262,1023  
 White S D M .and Frenk C . (1993) A strophys. J. 379,52  
 Wolfe A ., in Relativistic Astrophysics and Particle Cosm ology, ed. A ckerolf  
 C W .and Srednicki M A . (New York Acad. Sci., New York, 1993)  
 Zabludo A .I., Huchra J P .and G eller M J. (1990) A strophys. J. S. S. 74, 1

## FIGURE CAPTIONS

Fig. 1 { The curves enclose areas where models predict LSS linear features consistent with observations. Each curve refers to the value of  $n$  written aside. Point {dashed lines refer to models with HDM made of massive  $\nu$ 's. See the text for a more detailed comparison of the LSS they predict with volatile models. In g. 1a the constraints taken into account are: cluster abundance,  $\sigma_8$  value, gas in damped Ly $\alpha$  systems. In g. 1b the value of the extra power parameter  $\beta$  is also constrained.

Fig. 2 { Mixed model spectra with volatile hot component (solid line), compared with standard CDM (dotted line). The LCRS reconstructed spectrum is also reported (3 errorbars). Models a;b;c are consistent with all constraints. Model d is outside the contours plotted in g. 1b and has a small  $\beta$ . Models like it would agree with data for a still greater  $n$ .

Fig. 3 { Mixed model spectra, with thermal hot component (solid line) compared with standard CDM (dotted line) and LCRS reconstructed spectrum, as in g. 2. Models a;b agree with all constraints. Model c is in marginal disagreement, in spite of adding extra SMLC amounting to 3 massless  $\nu$ 's.

## Appendix A

In the decay  $X \rightarrow \nu + \gamma$ , both  $\nu$  and  $\gamma$  acquire momentum (and energy)  $p_{in} = m_X/2$ . If a decay occurs at  $t_p$ , at any later  $t$ , the momentum is redshifted into  $p = p_{in} a(t_p)/a(t)$ ; in turn this means that, at any  $t$ , a  $\nu$ {particle of momentum  $p$  was born when the scale factor was

$$a(t_p) = a(t) 2p/m_X : \quad (a1)$$

The map of  $p$  on  $a(t_p)$  yields that  $2a(t)/m_X = a(t_p)/p$  and

$$dp = d[a(t_p)] = m_X/2a(t) = p/a(t_p) : \quad (a2)$$

This allows to give the momentum distribution of  $\nu$ {particles

$$\nu(p) = \frac{1}{N_\nu} \frac{dN_\nu}{dp} = \frac{a(t_p)/a(t)}{p} \exp\left(-\frac{t_p}{t}\right) \quad (a3)$$

when the decay is complete. In fact, using (a2),  $dN_\nu = dp = [dN_\nu/dt_p] [dt_p/da(t_p)] [da(t_p)/dp] = [N_\nu/t_p] [1/a(t_p)] [a(t_p)/p]$ .

The expression (a3) is greatly simplified if the expansion is radiation dominated during the decay. In such a case  $a(t_p) = a(t) \sqrt{2t_p/t}$ , while, using eq. (a1),

$$Q = t_p/t = [a(t_p)/a(t)]^2 = (p/p_0)^2 \quad (a4)$$

with

$$p_0 = (m_X/2) [a(t_p)/a(t)] : \quad (a5)$$

Accordingly,

$$\nu(p) = 2(Q/p_0) \exp(-Q) : \quad (a6)$$

Henceforth, at large  $p$ , the distribution decays as  $\exp(-p^2/p_0^2)$ . Large  $p$  come from late decays, when the decay process is however radiation dominated; therefore the latter property is always true.

Owing to eq. (a4)

$$dQ = Q = 2 dp/p \quad (a7)$$

and, therefore,  $\nu$  can be easily verified to be normalized to unity. In a similar way

$$\int_0^\infty dp p \nu(p) = 2 p_0 \int_0^\infty dx x^2 \exp(-x^2) = p_0^2/2 \quad (a8)$$

This allows to replace, in the definition (a5) of  $p_0$  and, henceforth, in the distribution  $\nu$ , parameters referring to the decay process ( $m_X$  and  $t_p$ ) with parameters explicitly related to a cosmological model: the derelativization time/redshift/scale factor (subscript  $der$ ) and the  $\nu$ {particle mass  $m$ . By definition, let the derelativization occur when  $hpi = m$  or, according to eq. (a8), when  $p_0^2 = 2m^2$ . Then, at any time:

$$p_0 = (2m^2)^{1/2} (a_{der}/a) : \quad (a5^0)$$



Henceforth, the distribution peak and cut-off move towards smaller energies as the Universe expands, with  $\rho a = \text{const.}$

In Appendix B, we discuss the time evolution of a model. The basic reference redshift will be  $z_{\text{eq}} = 10^4$ . If  $\Omega = T_0 = 2.7333 \text{ K} = 1$ , the present radiation density  $\rho_{\text{cr}} = \rho_{\text{eq}}$ .

In respect to  $z_{\text{eq}}$  let us define:  $z_{\text{eq}} = z_{\text{der}}, y = a_{\text{eq}}/a = (1+z)^{-4} = 10^{-4}$ . It will be:

$$h_i = m y d \quad \text{and} \quad p = m y d 2^{\frac{p}{2}} : \quad (\text{a9})$$

In the case of HDM made of massive  $\nu$ 's, the momentum distribution reads:

$$(p) = [2=3 (3)] [p=T]^3 [p(e^{\frac{p}{T}} + 1)]^{-1} \quad (\text{n6})$$

and, accordingly,

$$h_i = [7^{-4} = 180 (3)] T \quad (\text{n8})$$

Eq. (n6) shows that, for large  $p$ , such distribution decays  $\sim \exp(-p)$ .

Furthermore,  $\nu$ 's become non-relativistic when  $T = m 180 (3) = 7^{-4}$  and, while the former equation (a9) still holds, it is

$$T = m y d 180 (3) = 7^{-4} : \quad (\text{n9})$$

Let us now show that

$$h = h_d \quad \text{at high } z: \quad (\text{a10})$$

At such  $z$ 's, in fact,  $h_i = h_i$  can be expressed through eq. (a9). In turn, the number density can be obtained rescaling its value at  $z = 0$ . Henceforth

$$n = m y d n_h = m y d \frac{h_{\text{cr}}}{m} \frac{a_0^3}{a} = h_d \frac{a_{\text{eq}}}{a_0} \frac{a_0^4}{a} \quad (\text{a11})$$

and, owing to the definition of  $a_{\text{eq}}$ , this shows (a10).

Let us now consider the constraints to a volatile model when  $\rho_{\text{early}}$ . The photon density before decay ( $\rho_{\text{early}}$ ) has safe lower limits related to BBNS, that we shall not discuss here; a fresh component, whose density coincides with  $\rho_h$ , accretes onto it because of the decay; hence, at any time,  $\rho > \rho_h$  and, owing to eq. (a10),

$$h_d \ll 1 \quad \text{for decay:} \quad (\text{a12})$$

Under such condition, it is almost granted that no matter dominance occurs, during the decay process. The actual constraint for this not to happen is that

$$h_d [1 + 2 = (1 + g = 8.3)]^{-1} \quad \text{for decay:} \quad (\text{a13})$$

In fact, comparing densities before and after decay, we have that the top value of  $x \sim 2 \rho_h$  and  $\rho_{\text{early}} \sim \rho_h$ ; furthermore  $w = w_0$  early with  $w_0 =$

$(4=11)^{4=3} g_{\nu}=16$  '  $g_{\nu}=8:8$  ( $g_{\nu}$  are the spin states of massless  $\nu$ 's). The requirement that the top value of  $x < x_{\text{early}} + \dots$ , yields  $2 h < (1 + w_o) (h)$  and hence, owing to eq. (a10),  $h d < [1 + 2(1 + w_o)]^{-1}$ . E.g.; for  $g_{\nu} = 6$ , eq. (a13) yields  $h d < 0.46$ .

Let us now consider the case of massless sterile scalar  $\nu$ 's. Arguments similar to those leading to eq. (a13) assure no matter domination before  $z_{\text{dy}}$  if

$$h d < (1 + w_o) = 2 \quad (\text{for sterile decay}): \quad (\text{a14})$$

In fact, in this case, the cosmological effects of  $\nu$ 's add to those of massless  $\nu$ 's and we shall therefore distinguish the real density  $\rho$  from the effective density

$$\rho = \rho_{\nu} + \dots = w \quad (\text{a15})$$

where  $w = w_o + h d$ . Once again, the top value of  $x$  is  $2 h$  and, in order that, at all times,  $x < (1 + w_o)$ , owing to eq. (a10), eq. (a14) must be fulfilled. The increase of the radiative sterile component can be also expressed renormalizing  $g_{\nu}$  into

$$g_{\text{eff}} = g_{\nu} + 8.80640 h d \quad (\text{a16})$$

which coincides with eq. (2.14).

Let us then discuss where the actual equivalence redshift  $z_{\text{eq}}$  is set. If  $\nu$  particles do not contribute to the relativistic component,

$$z_{\text{eq}} = z_{\text{cr}} = (1 + w) = z_{\text{eq}} = (1 + w)^{-4} \quad (\text{a17})$$

If  $z_{\text{der}} < z_{\text{eq}}$ , as is defined here, i.e.: if  $d(1 + h) > 1 + w_o$ ,  $\nu$ 's are to be added to the relativistic component and

$$z_{\text{eq}} = z_{\text{eq}} (1 + h) = (1 + w_o + 2 h d)^{-4} : \quad (\text{a18})$$

## Appendix B

The system of equations to be integrated in order to work out fluctuation evolution has been discussed in many papers. E.g.; an excellent and updated discussion is given by Ma & Bertschinger (1996). Here we shall report only the changes needed to treat HDM, if it is made of  $\nu$  particles.

Let the phase space distribution be  $f = f_o (1 + \dots)$ . For massive  $\nu$ 's

$$f_o = (2\pi)^{-3} g (e^x + 1)^{-1} \quad \text{with} \quad x = p/T \quad (\text{n1})$$

and, therefore, the expression

$$(x=f_o) (\partial f_o / \partial x) = -x = -(1 + e^x) \quad (\text{n2})$$

will enter the equation (b3) here below. For volatiles, instead,

$$f_o = (2)^{-1} N_v (a_o = a_p)^3 Q e^{-Q} \quad (b1)$$

and

$$(a_p = f_o) (\partial f_o = \partial a_p) = (1 + 2Q) \quad (b2)$$

will be used in the equation:

$$\frac{\partial}{\partial t} + \frac{i p}{E} k \frac{a_o}{a} + \frac{1}{4} H \frac{a_p}{f_o} \frac{\partial f_o}{\partial a_p} = 0 \quad (b3)$$

where  $k$  is the wave{number of the perturbation,  $H$  accounts for the gravitational interaction and yields the angle dependence of . It should also be outlined that, while for massive 's,  $p = E [1 + 1 = x^2 y^2 d^2]^{1=2}$ , with  $d = d180 (3) = 7^{-4}$ , here

$$\frac{p}{E} = 1 + \frac{1}{Q y^2 d_v^2} \quad (b4)$$

with  $d_v = d2 = \frac{p}{E}$ .

The different phase{space distribution has further effects on the gravitational field equations, that we treated in the synchronous gauge. Here we consider the stress{energy tensor  $T_{ij}$  for massive 's and its perturbation

$$(2T_{00} - T) = d^3 p E (1 - m^2 = 2E^2) f_o; \quad (n4)$$

where  $f_o$  is the 0{th order term in a spherical harmonic expansion of . As  $E (1 - m^2 = 2E^2) = m (1 = 2 + x^2 y^2 d^2) = (1 + x^2 y^2 d^2)^{1=2}$  it turns out that

$$(2T_{00} - T) = \frac{1}{2} \text{cr}_h z_{eq}^3 y^3 e_3; (y d) \quad (n5)$$

with

$$e_3; (s) = 2 \int_0^{\frac{1}{2}} dx e^{-x} (x) \frac{1=2 + s^2 x^2}{(1 + s^2 x^2)^{1=2}} \quad (n5^0)$$

where  $(x) = x^2 = (1 + e^{-x})$ . For volatiles we have an analogous expression:

$$(2T_{00} - T) = \frac{1}{2} \text{cr}_h z_{eq}^3 y^3 e_{3,v} (y d) \quad (5b)$$

with

$$e_{3,v} (s) = 2 \int_0^{\frac{1}{2}} dQ e^{-Q} \frac{1=2 + s^2 Q}{(1 + s^2 Q)^{1=2}} \quad (b5^0)$$

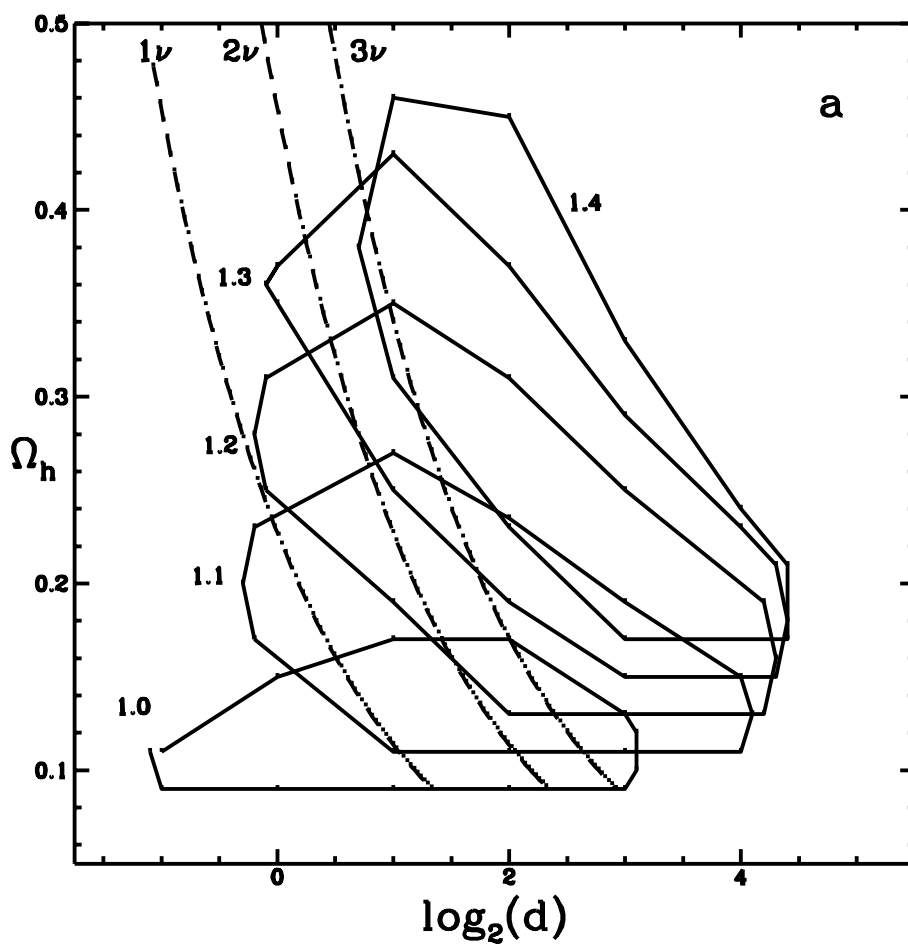
In the gravitational field equations also the quantity  $e_4 = \int_0^{R_1} dx e^{-x} x (x)_{-1} (x)$  is used, for massive 's ( $_{-1}$  is the first order term in the spherical harmonic expansion of ). For volatiles it ought to be replaced by

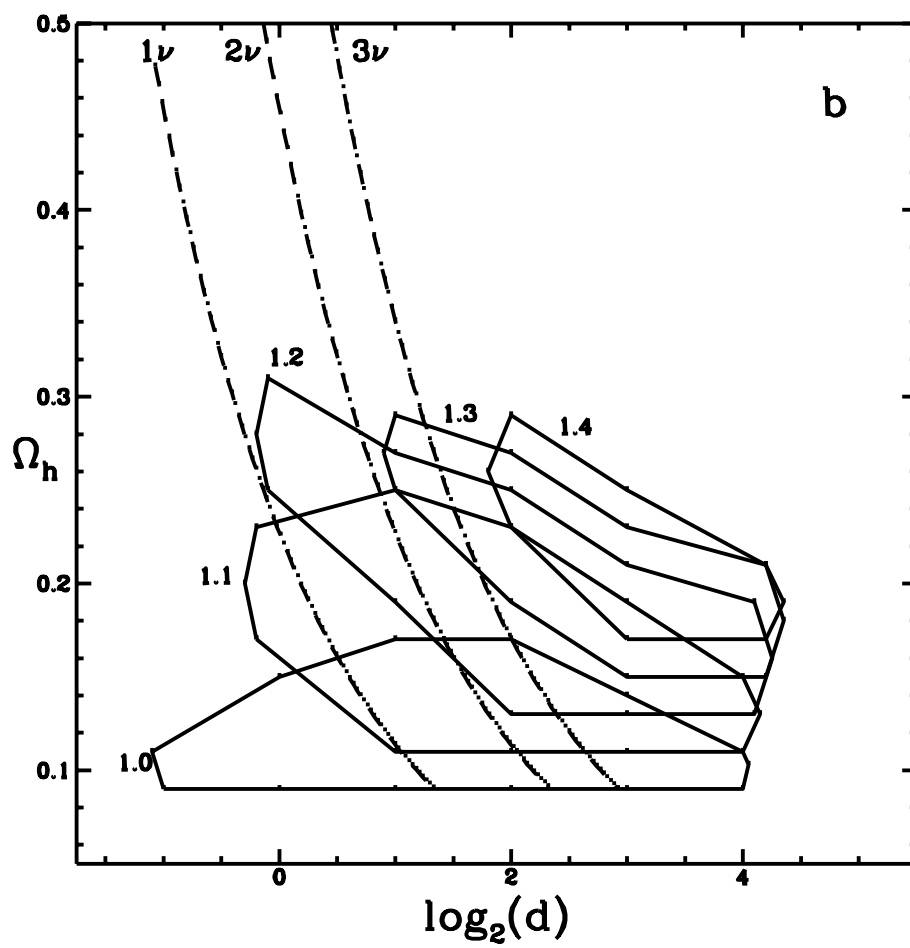
$$e_{4,v} = \int_0^{\frac{1}{2}} dQ e^{-Q} \frac{q}{Q_{-1} (Q)} : \quad (b6)$$

Our code integrates the set of equations for the fluctuation evolution in the synchronous gauge. We speed it up by truncating the hierarchical set of equations of free-streaming particles (photons after recombination, HDM and massless  $\nu$ 's), according to the scheme suggested by Ma & Bertschinger (1996), slightly modifying it because we don't use conformal time. Results with truncation were compared with results with a free number of harmonics and we found that a truncation at the 8th harmonics is mostly sufficient. Results presented here are however obtained with truncation at the 24th harmonics. Models were evolved down to  $z = 0$ . We evaluated the transfer function for 24 scales ranging from  $L = 20000 \text{ Mpc}$  to  $L = 0.53054 \text{ Mpc}$ . Results from the public code CMBFAST, yielding the transfer function for mixed models (only with thermal hot component), were compared with the results of our algorithm, for a number of models and for scales fixed by CMBFAST.

Relative discrepancies between code outputs vary from less than  $10^{-4}$ , on scales above  $100 \text{ Mpc}$ , to slightly above 3% in the worst cases, which occur for the hot component, when  $\Omega_h > 0.3$  and for scales below  $2.3 \text{ Mpc}$ . In such cases CMBFAST tends to give a transfer function slightly smaller than our code. The typical discrepancy, however, keeps safely below 0.5% and, therefore, we fully confirm the validity of CMBFAST.

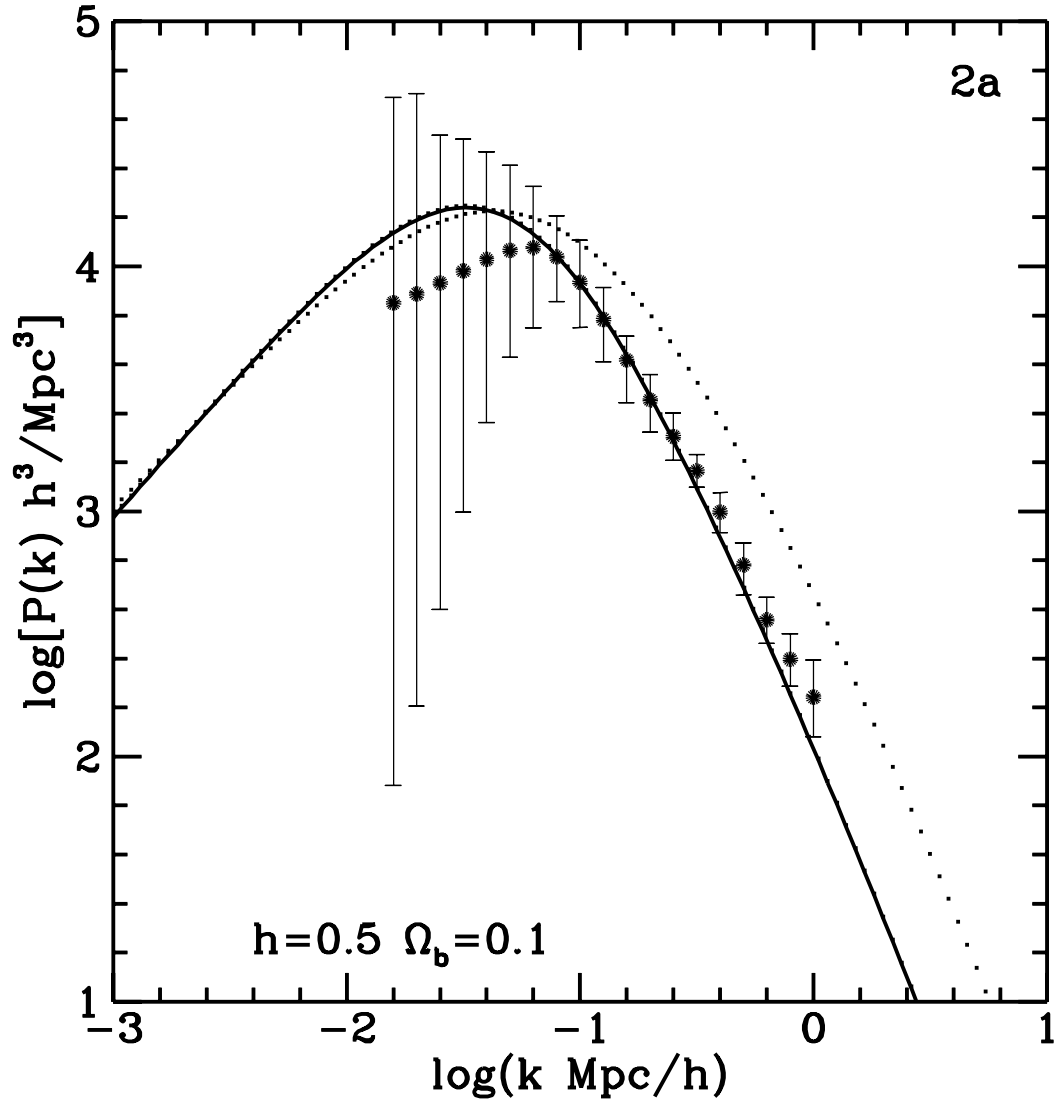
Altogether the main source of error comes from the analytic fit to the transfer functions, although the top discrepancy at a single point keeps  $< 1\%$  in the worst cases and its typical value is  $< 0.1\%$ .





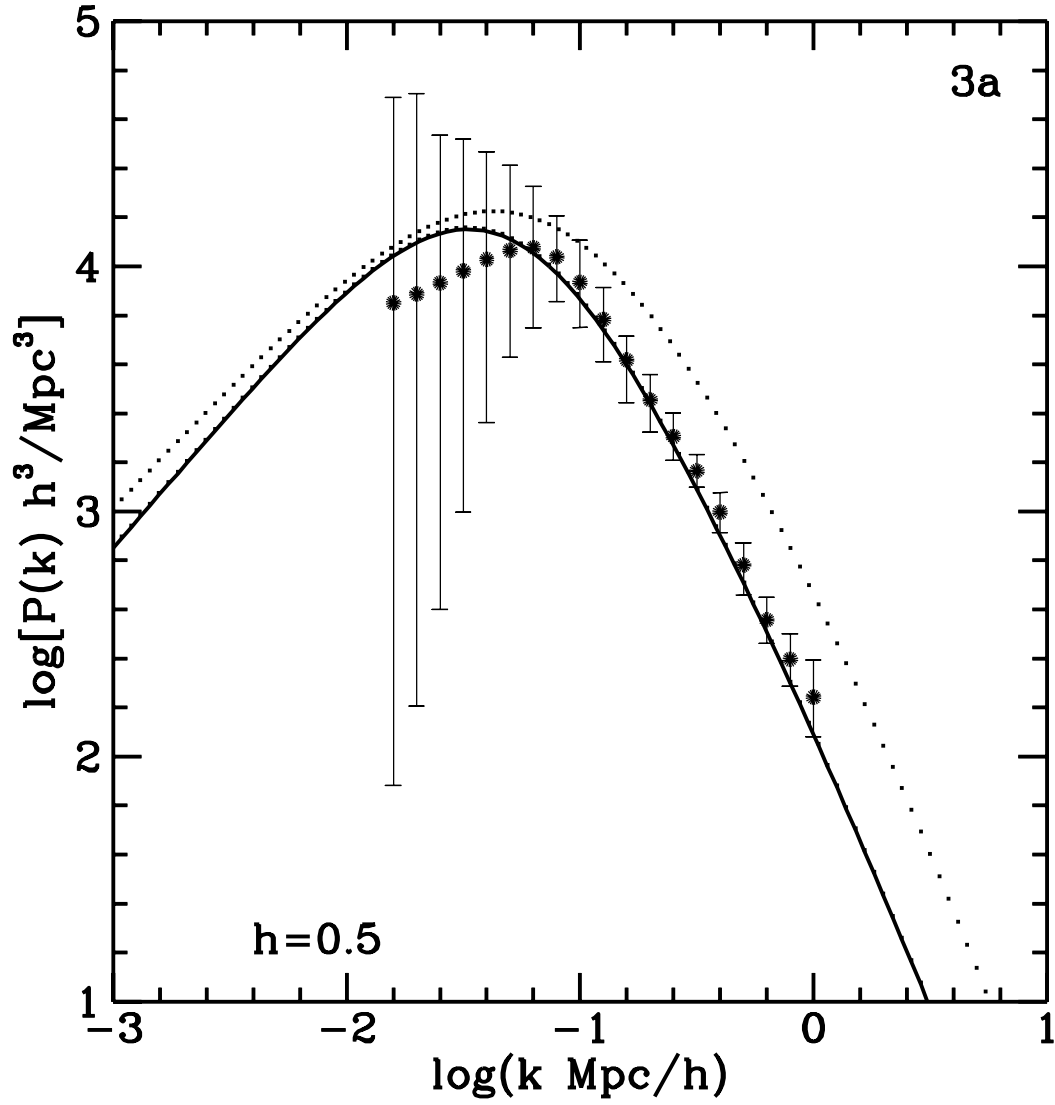
CDM:  $Q=15.7\mu\text{K}, n=1, N_{\text{cl}}=43, \Omega_{\text{g}}=23, \Gamma=0.42$

MDM:  $Q=14.2\mu\text{K}, n=1.1, \Omega_{\text{h}}=0.16, z_{\text{der}}=5000$   
 $N_{\text{cl}}=8-13, \text{DLAS}=1.2, \Gamma=0.20, \sigma_{\text{g}}=0.67$



CDM:  $Q=15.7\mu\text{K}, n=1, N_{\text{cl}}=43, \Omega_{\text{g}}=23, \Gamma=0.42, \Omega_{\text{b}}=0.1$

MDM:  $Q=12.3\mu\text{K}, n=1.1, \Omega_{\text{h}}=0.16, g_{\nu}=6, \Omega_{\text{b}}=0.09$   
 $N_{\text{cl}}=7-12, \text{DLAS}=3.7, \Gamma=0.23, \sigma_{\text{g}}=0.65$

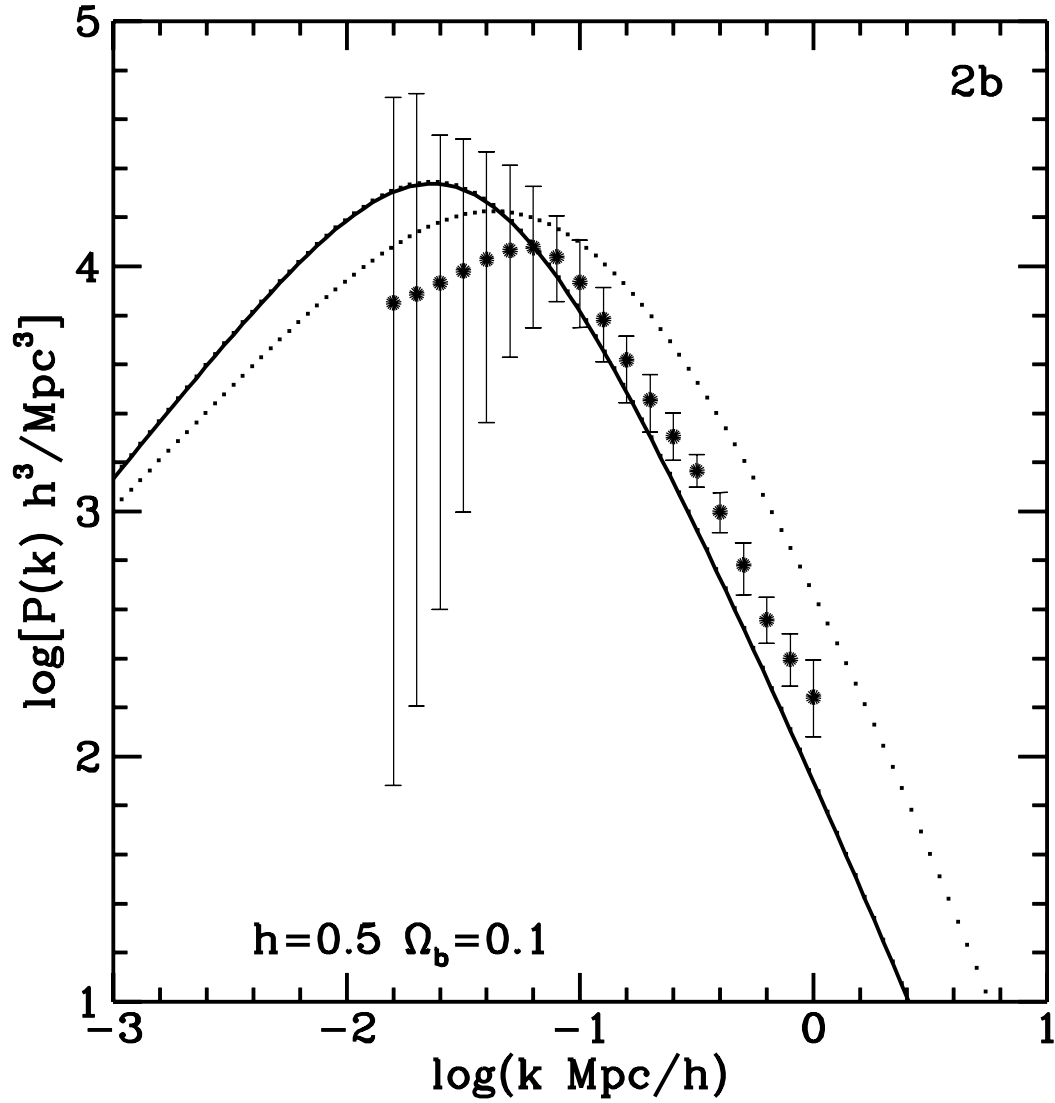




CDM:  $Q=15.7\mu\text{K}, n=1, N_{\text{cl}}=43, \Omega_g=23, \Gamma=0.42$

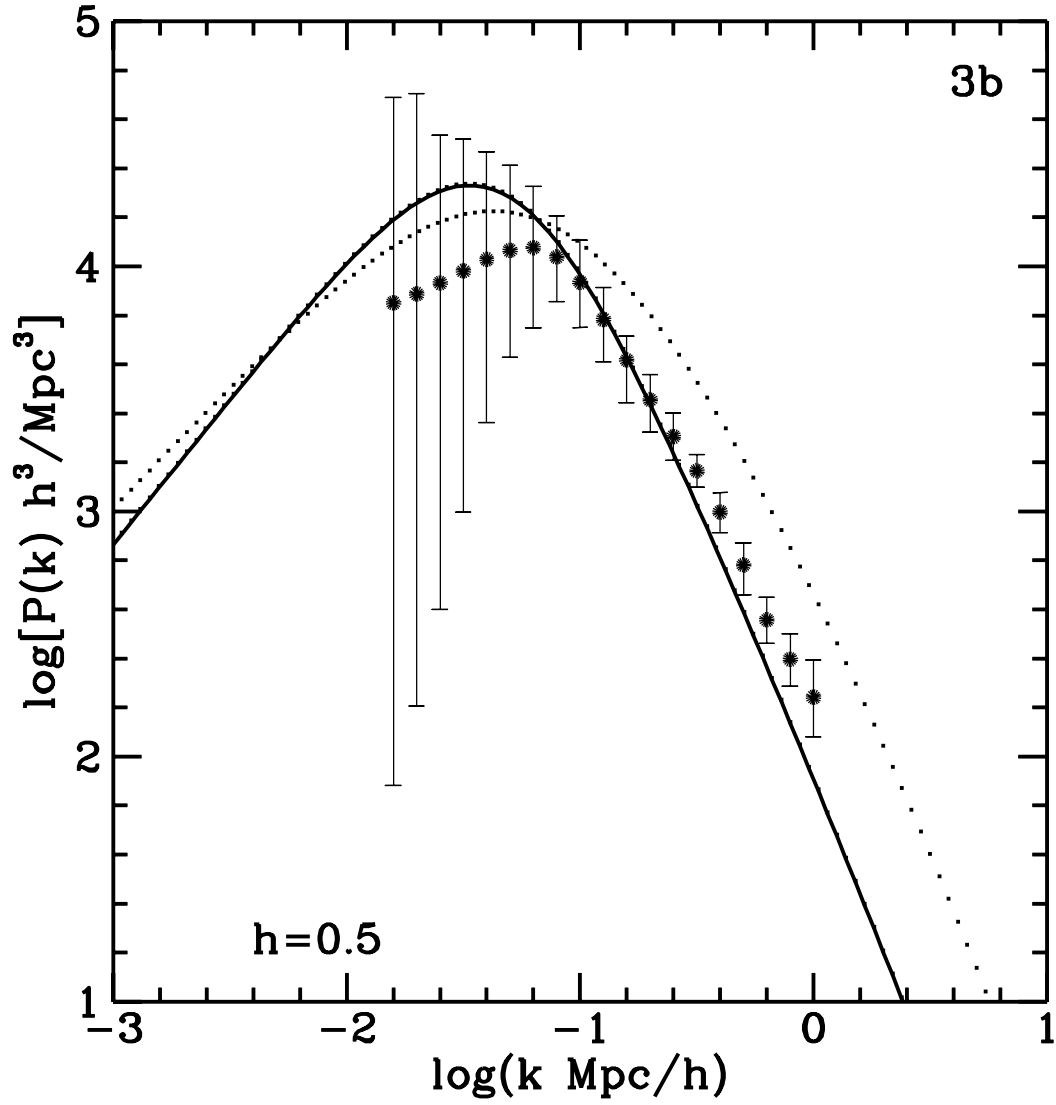
MDM:  $Q=16.0\mu\text{K}, n=1.2, \Omega_h=0.18, z_{\text{der}}=1250$

$N_{\text{cl}}=2.3-4.4, \text{DLAS}=0.7, \Gamma=0.15, \sigma_8=0.56$



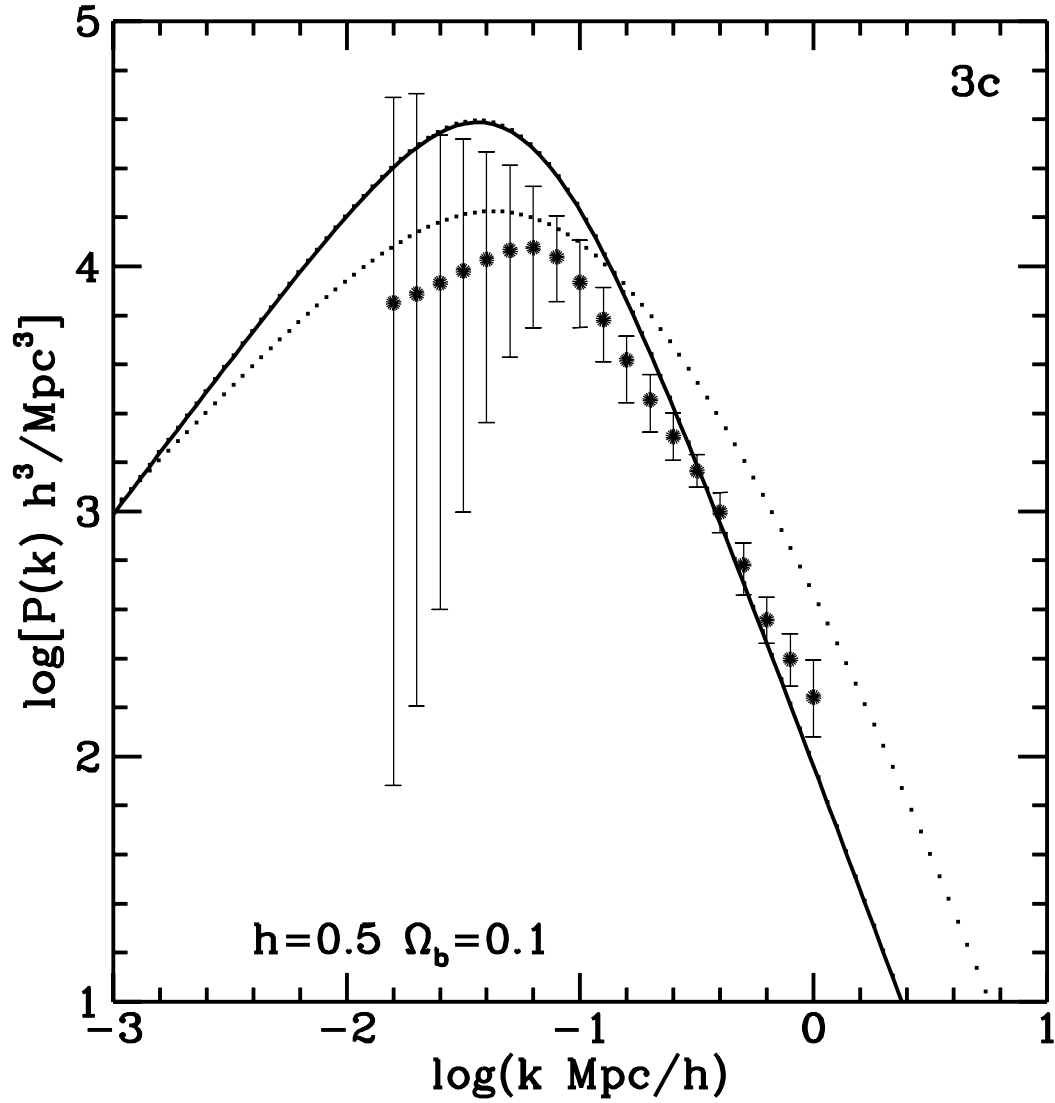
CDM:  $Q=15.7\mu\text{K}, n=1, N_{\text{cl}}=43, \Omega_{\text{g}}=23, \Gamma=0.42, \Omega_{\text{b}}=0.1$

MDM:  $Q=12.6\mu\text{K}, n=1.2, \Omega_{\text{h}}=0.27, g_{\nu}=6, \Omega_{\text{b}}=0.09$   
 $N_{\text{cl}}=6-10, \text{DLAS}=0.8, \Gamma=0.16, \sigma_{\text{g}}=0.65$



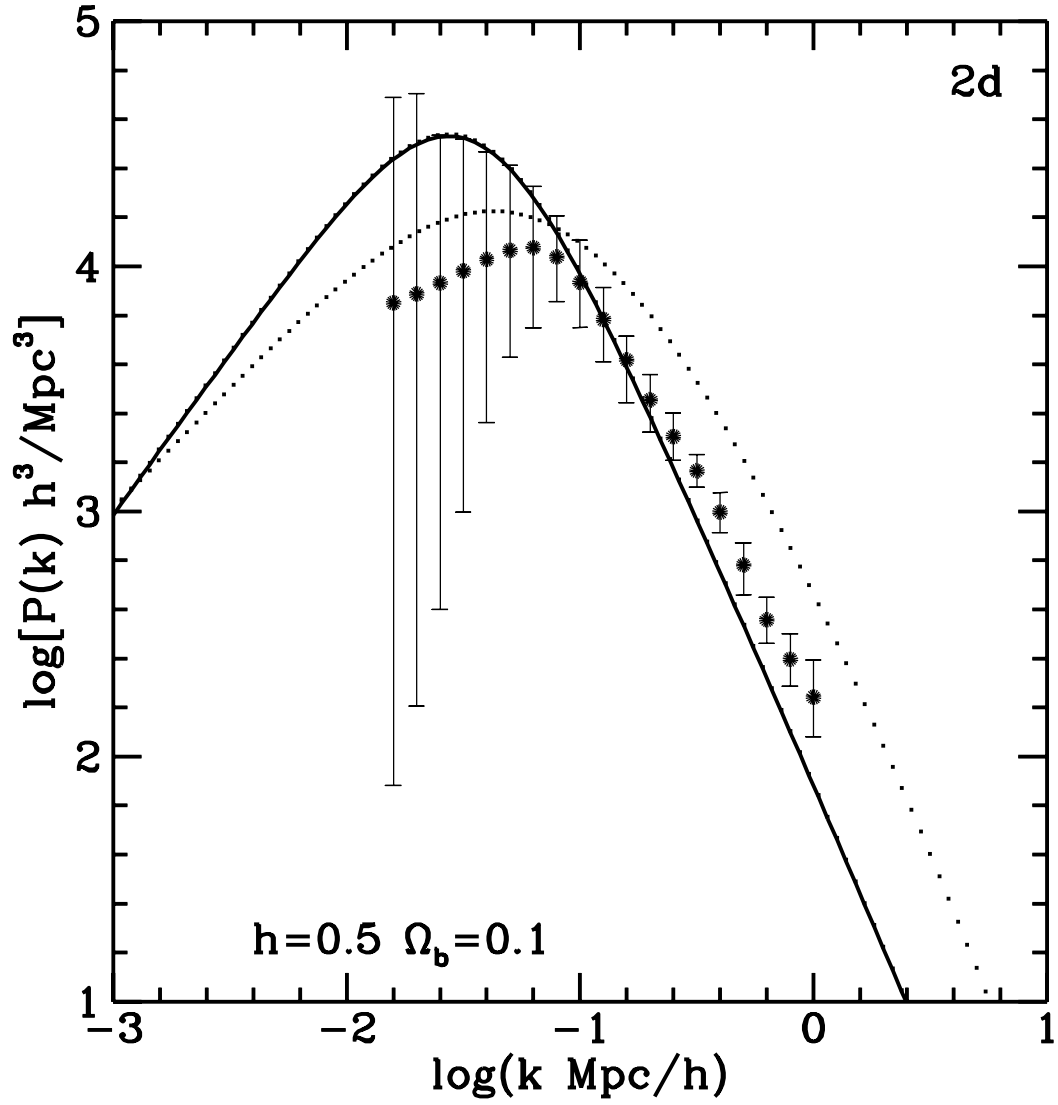
CDM:  $Q=15.7\mu\text{K}, n=1, N_{\text{cl}}=43, \Omega_g=23, \Gamma=0.42$

MDM:  $Q=12.6\mu\text{K}, n=1.3, \Omega_h=0.33, g_\nu=4$  (+SMLC)  
 $N_{\text{cl}}=17-23, \text{DLAS}=0.5, \Gamma=0.14, \sigma_8=0.80$



CDM:  $Q=15.7\mu\text{K}, n=1, N_{\text{cl}}=43, \Omega_g=23, \Gamma=0.42$

MDM:  $Q=11.3\mu\text{K}, n=1.4, \Omega_h=0.30, z_{\text{der}}=2500$   
 $N_{\text{cl}}=3.2-5.7, \text{DLAS}=0.7, \Gamma=0.11, \sigma_8=0.59$



CDM:  $Q=15.7\mu\text{K}, n=1, N_{\text{cl}}=43, \Omega_g=23, \Gamma=0.42$

MDM:  $Q=16.1\mu\text{K}, n=1.4, \Omega_h=0.22, z_{\text{der}}=625$   
 $N_{\text{cl}}=1.3-3.6, \text{DLAS}=2.8, \Gamma=0.13, \sigma_8=0.54$

